

# Dissipation induced Majorana 0- and $\pi$ -modes in a driven Rashba nanowire

Koustabh Gogoi <sup>1</sup>, Tanay Nag <sup>1,\*</sup> and Arnob Kumar Ghosh <sup>2,†</sup>

<sup>1</sup>*Department of Physics, BITS Pilani-Hyderabad Campus, Telangana 500078, India*

<sup>2</sup>*Department of Physics and Astronomy, Uppsala University, Box 516, 75120 Uppsala, Sweden*

Periodic drive is an intriguing way of creating topological phases in a non-topological setup. However, most systems are often studied as a closed system, despite being always in contact with the environment, which induces dissipation. Here, we investigate a periodically driven Rashba nanowire in proximity to an  $s$ -wave superconductor in a dissipative background. The system's dynamics is governed by a periodic Liouvillian operator, from which we construct the Liouvillian time-evolution operator and use the third-quantization method to obtain the 'Floquet damping matrix', which captures the spectral and topological properties of the system. We show that the system exhibits edge-localized topological Majorana 0-modes (MZMs) and  $\pi$ -modes (MPMs). Additionally, the system also supports a trivial 0-modes (TZMs) and  $\pi$ -modes (TPMs), which are also localized at the edges of the system. The MZMs and the MPMs are connected to the bulk topology and carry a bulk topological invariant, while the emergence of TZMs and TPMs is primarily tied to exceptional points and is topologically trivial. We study the topological phase diagrams in terms of the topological invariants and show that the dissipation can modify the topological phase diagram substantially and even induce topological phases in the system. Our work extends the understanding of a driven-dissipative topological superconductor.

## I. INTRODUCTION

The search for Majorana zero-modes (MZM) in topological superconductors (TSCs) has engaged physicists for the past two decades [1–7]. The seminal proposition for realizing Majorana in a condensed matter system, proposed first by Kitaev, is based on  $p$ -wave superconductor [1]. However, the  $p$ -wave superconductors do not emerge naturally. Nevertheless, we can still engineer an effective  $p$ -wave superconductor from a conventional  $s$ -wave superconductor by employing a semiconducting nanowire with Rashba spin-orbit coupling (SOC) and a Zeeman field [3, 4, 6, 8–11]. Although, the experimental evidence of detecting MZM in this heterostructure setup remain elusive [10–22]. Nonetheless, a simpler and more controllable setup to realize so-called “poor man’s” MZMs without any topological protection and based on the Kitaev model has attracted a lot of attention recently [23, 24].

At the same time, the quest for TSC has been further enriched in periodically driven systems, allowing us to engineer a non-trivial phase in an otherwise trivial system [25–36]. Moreover, the driven system also offers topologically protected Majorana states at a finite quasienergy  $E = \omega/2$  ( $\omega$  is the frequency of the drive), which are called Majorana  $\pi$ -modes (MPMs) [31–35]. These MPMs with the concurrent MZMs offer more flexibility in topological quantum computations [37, 38]. The MZMs and MPMs in a driven system have also been explored in the presence of non-Hermitian (NH) effects [39, 40]. The NH system offers many exotic behaviors that are absent in their Hermitian counterparts, such

as the breakdown of conventional bulk boundary correspondence [41–44], NH skin effects [43–47], the emergence of exceptional points (EPs) [43, 44, 47–53], and non-trivial behavior in dynamical quantum phase transition [54, 55]. Moreover, the NH-terms can substantially modify the topological phases in both driven and undriven systems [40, 41, 56].

The NH effect can enter a system in many different ways, but the dissipation via the coupling with the environment offers an intriguing way of obtaining the NH effect in a system [57–61]. While the dissipation can have a detrimental effect on the system and can manipulate the system's topological properties [62–72]. On the other hand, specifically engineered dissipation has been employed to obtain a topological phase out of a trivial system [73–82]. In a dissipative system, the system's long-time evolution is governed by the density matrix, and in the Markovian approximation of a memoryless bath [74, 83], the density matrix is governed by the Liouvillian operator, which follows the Lindblad master equation [84, 85]. Moreover, by employing the third-quantization method for linear jump operators, we can obtain a matrix form of the Liouvillian operator, which behaves like the NH Hamiltonian [86–88]. A topological classification based on the Liouvillian has also been investigated [63].

In this context, the MZMs and MPMs in a driven system are usually studied as a closed system. However, the system is often in contact with the surroundings, introducing some amount of dissipation [83, 89]. On the other hand, the dissipation offers a way of engineering the NH effect in a driven system [58, 82]. Recently, an open Rashba nanowire coupled with the environment has been studied in the presence of dissipation, while it has also been demonstrated that the dissipation can lead to the emergence of MZMs in such a system [82]. Motivated by this, we ask the following interesting questions:

\* Corresponding author: [tanay.nag@hyderabad.bits-pilani.ac.in](mailto:tanay.nag@hyderabad.bits-pilani.ac.in)

† Corresponding author: [arnob.ghosh@physics.uu.se](mailto:arnob.ghosh@physics.uu.se)

(a) Can the MZMs and MPMs be obtained in a driven-dissipative Rashba nanowire? (b) Can the dissipation even assist in obtaining topological phases that are not present in the non-dissipative case? In this manuscript, we affirmatively answer these questions.

In this work, we consider a three-step driving protocol in a Rashba nanowire, which is coupled with the environment via linear jump operators. We employ the third-quantization method and obtain a Floquet Liouvillian [58, 86–88]. We demonstrate that the dissipation offers an exotic way of obtaining and understanding the NH effect in a driven system where MZMs and MPMs can be engineered. Surprisingly, we also find some boundary modes appearing at both 0- and  $\pi$ -quasienergy, dubbed as trivial 0-modes (TZMs) and  $\pi$ -modes (TPMs) respectively, that are not protected by the bulk gap but rather induced by the EPs. We also investigate the eigenvalue spectra and the edge-localization properties of the states appearing at quasienergies  $0, \pm\pi$ . While the TZMs and TPMs do not carry any topological indices, we topologically characterize the MZMs and MPMs employing winding numbers based on a generalized chiral symmetry and obtain a phase diagram in the parameter space. This phase diagram also points out the non-trivial generation of MZMs and MPMs in a dissipative system.

The remainder of the manuscript is organized as follows. In Sec. II, we discuss the model Hamiltonian for the Rashba nanowire and introduce the driving protocol. In Sec. III, we discuss the form of dissipation, the third-quantization method to obtain the Floquet Liouvillian, and the real space topological invariant to characterize the system. Section V presents the main results of this work. We conclude with a summary and discussion in Sec. VI.

## II. MODEL AND DRIVING PROTOCOL

We consider a Rashba nanowire in proximity to a bulk  $s$ -wave superconductor in the presence of an in-plane magnetic field. The Hamiltonian of this system reads as [3, 4, 6, 8–11]

$$H_0 = -\mu \sum_{i=1}^N \sum_{\alpha=\uparrow,\downarrow} c_{i\alpha}^\dagger c_{i\alpha} + t_h \sum_{i=1}^{N-1} \sum_{\alpha=\uparrow,\downarrow} c_{i\alpha}^\dagger c_{i+1\alpha} - i\lambda_R \sum_{i=1}^{N-1} \sum_{\alpha,\beta=\uparrow,\downarrow} c_{i\alpha}^\dagger (\sigma_z)_{\alpha,\beta} c_{i+1\beta} + B \sum_{i=1}^N \sum_{\alpha,\beta=\uparrow,\downarrow} c_{i\alpha}^\dagger (\sigma_x)_{\alpha,\beta} c_{i\beta} + \Delta \sum_{i=1}^N c_{i\uparrow}^\dagger c_{i\downarrow}^\dagger + \text{H.c.}, \quad (1)$$

where  $\mu$ ,  $t_h$ ,  $\lambda_R$ ,  $B$ , and  $\Delta$  represent onsite chemical potential, hopping amplitude, Rashba SOC strength, in-plane magnetic field along  $x$ -direction, and proximity induced  $s$ -wave pairing gap, respectively. Here,  $c_{i\alpha}$  ( $c_{i\alpha}^\dagger$ ) creates (annihilates) an electron at lattice site  $i$  with spin  $\alpha = \uparrow, \downarrow$ , and  $N$  denotes the number of lattice sites in the

system. The Pauli matrices  $\sigma$  act on the spin space. For an infinite and translation-invariant nanowire, we can write the Hamiltonian of the system in the momentum space considering the Bogoliubov-de Gennes basis  $\Psi_{\mathbf{k}} = \{c_{k\uparrow}, c_{k\downarrow}, -c_{-k\downarrow}^\dagger, c_{-k\uparrow}^\dagger\}^T$  as

$$H_0(k) = (-\mu + 2t_h \cos k) \tau_z \sigma_0 + 2\lambda_R \sin k \tau_z \sigma_z + B \tau_0 \sigma_x + \Delta \tau_x \sigma_0, \quad (2)$$

where the Pauli matrices  $\tau$  act on the particle-hole sector. The Hamiltonian [Eq. (2)] respects chiral symmetry  $SH_0(k)S = -H_0(k)$  with  $S = \tau_y \sigma_z$  and particle-hole symmetry  $C^{-1}H_0(k)C = -H(-k)$  with  $C = \tau_y \sigma_y K$ ;  $K$  being the complex-conjugation operator. However, the introduction of a magnetic field breaks the time-reversal symmetry  $\mathcal{T}^{-1}H(k)\mathcal{T} \neq H(-k)$  with  $\mathcal{T} = i\tau_0 \sigma_y K$ . The interplay of Rashba SOC, magnetic field, and the  $s$ -wave superconductivity induces an effective spin-triplet  $p$ -wave pairing in the nanowire [3, 4, 6, 8–11]. The system becomes topological supporting non-trivial MZMs when  $|B_{c1}| < B < |B_{c2}|$  with  $|B_{c1}| = \sqrt{(\mu - 2t_h)^2 + \Delta^2}$  and  $|B_{c2}| = \sqrt{(\mu + 2t_h)^2 + \Delta^2}$  [33]. We set  $2t_h = \lambda_R = \Delta = 1$  and  $\mu = 0$  throughout the manuscript unless mentioned otherwise. However, our results are independent of such a choice of the parameters.

To engineer the MZM and MPM in the Rashba nanowire, we consider a periodic drive in the form of a three-step drive protocol on top static Hamiltonian  $H_0$  as [33]

$$H(t) = \begin{cases} H_1 & t \in [0, T/4], \\ H_0 & t \in [T/4, 3T/4], \\ H_1 & t \in [0, T], \end{cases} \quad (3)$$

where the step Hamiltonians at the first and last step only comprise the onsite chemical potential, such that  $H_1 = -\mu_1 \sum_{i=1}^N \sum_{\alpha=\uparrow,\downarrow} c_{i\alpha}^\dagger c_{i\alpha}$ . In the absence of any loss in the setup, the spectral properties of the driven system is captured by the stroboscopic Floquet operator in the time-ordered (TO) notation as  $U(T, 0) = \text{TO} \exp[-i \int_0^T dt H(t)]$  [33, 90]. The Floquet operator follows the eigenvalue equation:  $U(T, 0)|\psi_n\rangle = \exp(-i\epsilon_n T)|\psi_n\rangle$ , where  $\epsilon_n$  is the quasienergy corresponding to the state  $|\psi_n\rangle$ . This system has been investigated in detail in Ref. [33] and has been shown to support both MZMs and MPMs.

## III. DISSIPATION AND FLOQUET LINDBLADIAN

To explore the effect of dissipation on the MZMs and MPMs, we couple our system to an environment. However, to study the driven system in a dissipative background, we need to formulate the Floquet formalism in such a way that it captures the effect of the environment.

In this section, we briefly discuss how to obtain the Floquet Liouvillian, which governs the dynamics of the system in the presence of dissipation [58, 91], employing the third-quantization method [86–88].

### A. Lindblad master equation and jump operator

We begin by discussing the effect of the dissipation on a static system. We adopt the Markovian approximation such that the time evolution of the density matrix  $\rho(t)$  is governed by the Lindblad master equation [74, 83–85]

$$\begin{aligned} \frac{\partial \rho(t)}{\partial t} &= -i[H, \rho(t)] - \frac{1}{2} \sum_m (\{L_m^\dagger L_m, \rho(t)\} - 2L_m^\dagger \rho(t) L_m), \\ &\equiv \mathcal{L}\rho(t), \end{aligned} \quad (4a) \quad (4b)$$

The first term in Eq. (4a) involving the Hamiltonian  $H$  generates a unitary evolution, while the second term associated with the Lindblad jump operator  $L_m$  accounts for the system's coupling to the reservoir. More precisely, the term  $\{L_m^\dagger L_m, \rho(t)\}$  is partially responsible for a non-unitary evolution of the system, while the term  $L_m^\dagger \rho(t) L_m$  is called the quantum jump [64], which mixes between different states of the system. Together, these operators form the Liouville operator  $\mathcal{L}$ , which governs the dynamics of the system.

The Lindblad jump operator can have different forms, but for simplicity, we consider an onsite loss operator in terms of a linear combination of fermionic annihilation operators only, which at a lattice site  $i$  reads as

$$L_i = \sqrt{\gamma} (c_{i\uparrow} + c_{i\downarrow}), \quad (5)$$

where  $\gamma$  denotes the strength of the dissipation. The loss operator  $L_i$  acts on both spin species [82]. The linear jump operators in Eq. (5) allow us to obtain a matrix form of the Liouvillian  $\mathcal{L}$ , utilizing the third-quantization method [86–88].

### B. Third quantization

Here, we briefly discuss the third-quantization method [86–88]. First, we replace the complex fermionic operator with real Majorana fermions as  $c_{i\uparrow} = (w_{iA} + iw_{iB})/2$  and  $c_{i\downarrow} = (w_{iC} + iw_{iD})/2$  such that the Majorana operators satisfy the anti-commutation rule:  $\{w_{i\alpha}, w_{j\beta}\} = 2\delta_{i,j}\delta_{\alpha,\beta}$ ; with  $\alpha = A, B, C, D$  and  $i, j = 1, 2, \dots, N$ . The Hamiltonian  $H$  and the Lindblad jump operators  $L_m$  can be written by employing the Majorana operators as  $H_M = \sum_{a,b}^{4N} w_a H_{a,b} w_b = \underline{w}^T H^{(w)} \underline{w}$  and  $L = \sum_a^{4N} l_a w_a = \underline{l} \underline{w}$ ; with  $\underline{w} = \{w_{1A}, w_{1B}, w_{1C}, w_{1D}, \dots, w_{iA}, w_{iB}, w_{iC}, w_{iD}, \dots\}^T$ . Next, we introduce a Fock space called the Liouville-Fock space  $\mathcal{K}$  spanned by the polynomial:  $P_\alpha = \prod_{a=1}^{4N} w_a^{\alpha_a}$ , with

$\alpha_a \in 0, 1$  representing the absence or presence of the Majorana operator  $w_a$ . The density matrix  $\rho(t)$  is a vector in this Fock space  $\mathcal{K}$ . Within this Fock space, we can define the adjoint fermion annihilation operator:  $\hat{\phi}_a |P_\alpha\rangle = \delta_{\alpha_a, 1} |w_a P_\alpha\rangle$  and creation operator:  $\hat{\phi}_a^\dagger |P_\alpha\rangle = \delta_{\alpha_a, 0} |w_a P_\alpha\rangle$ , such that  $\{\hat{\phi}_a, \hat{\phi}_b^\dagger\} = \delta_{a,b}$ . Now, assuming an even number of Majorana fermions in the system, such that we can recast them to obtain complex fermions without leaving any unpaired Majorana fermions. In the even subspace (+), the Liouvillian operator, denoted as  $\mathcal{L}_+$  can be put in the form [82, 86–88]

$$\mathcal{L}_+ = \frac{1}{2} \begin{pmatrix} \phi^\dagger & \phi \end{pmatrix} \begin{pmatrix} -iX^\dagger & Y \\ 0 & iX \end{pmatrix} \begin{pmatrix} \phi^\dagger \\ \phi \end{pmatrix} - A_0, \quad (6)$$

where  $X = 4H_M + i(M + M^T)$ ,  $Y = 2(M - M^T)$ , and  $A_0 = \frac{1}{2} \text{Tr}[X]$ , with  $M_{mn} = (l)_m^T (l)_n^*$ . The vectors  $\underline{\phi}_k^\dagger$  and  $\underline{\phi}_k$  contains  $\hat{\phi}_a^\dagger$ 's and  $\hat{\phi}_a$ 's, respectively. The operator  $X$  is also called the damping matrix. Owing to the upper triangular form of  $\mathcal{L}_+$ , the spectral and topological properties of the system are solely determined by  $X$  [63, 82]. Furthermore, the operator also resembles the NH Hamiltonians, but with a subtle difference that the imaginary eigenvalue of the  $X$  is always positive, such that the density matrix decays over time and reaches the steady state:  $\rho_{ss} = \exp[i\mathcal{L}_+ t] \rho(0)$ .

### C. Floquet-Liouvillian

Here, we discuss how we obtain the Floquet-Liouvillian operator, which governs the dynamics of a driven-dissipative system. In this regard, we consider that the driven Rashba nanowire setup is constantly in contact with the environment such that the dissipation of the form given in Eq. (5) is present in all the step Hamiltonians of Eq. (3). The description of the system involves a time-dependent periodic Liouvillian operator  $\hat{\mathcal{L}}(t)$ , and the Liouvillian time-evolution operator  $U_{\mathcal{L}}(T, 0)$  for this system can be constructed as [58]

$$U_{\mathcal{L}}(T, 0) = \text{TO exp} \left[ \int_0^T dt \hat{\mathcal{L}}(t) \right]. \quad (7)$$

Here,  $U_{\mathcal{L}}(T, 0)$  provides the stroboscopic description of the system in this driven-dissipative setup. We can obtain the Floquet Liouvillian  $\mathcal{L}_F$  as:  $U_{\mathcal{L}}(T, 0) = e^{\mathcal{L}_F T}$ . Now, considering the third-quantized Liouvillian operator [see Eq. (6)], we can obtain the Floquet Liouvillian as

$$U_{\mathcal{L}}(T, 0) = e^{\mathcal{L}_F T} = \begin{pmatrix} e^{-iX_F^\dagger T} & f(X, Y, T) \\ 0 & e^{iX_F T} \end{pmatrix}, \quad (8)$$

where the matrix  $X_F$  plays the same role as  $X$ , but for a driven system, while the function  $f(X, Y, T)$  is a complex function of  $X$  and  $Y$ . However, the Liouvillian

time-evolution operator  $U_{\mathcal{L}}(T, 0)$  being an upper triangular matrix, the spectral and topological properties of the system are governed by the ‘Floquet damping matrix’  $X_F$  alone, and henceforth we focus our discussion on  $X_F$ . The Floquet damping matrix  $X_F$  is the dynamical analog of the static damping matrix  $X$  defined in Eq. (6).

Having discussed the formalism, we now explicitly

show the form of the Floquet damping matrix  $X_F$  for our system. As discussed earlier, we allow the system to have dissipation in all the step Hamiltonians in Eqs. (3). Thus, the corresponding step damping matrices, written in the Majorana basis, owing to the dissipation of the form Eq. (5), read as

$$X_0 = \mu \sum_{i=1}^N \sum_{\alpha, \beta=1}^4 w_{i\alpha} (\tilde{\tau}_0 \tilde{\sigma}_y)_{\alpha, \beta} w_{i\beta} - t_h \sum_{i=1}^{N-1} \sum_{\alpha, \beta=1}^4 w_{i\alpha} (\tilde{\tau}_0 \tilde{\sigma}_y)_{\alpha, \beta} w_{i+1\beta} - i\lambda_R \sum_{i=1}^{N-1} \sum_{\alpha, \beta=1}^4 w_{i\alpha} (\tilde{\tau}_z \tilde{\sigma}_0)_{\alpha, \beta} w_{i+1\beta} \\ - B \sum_{i=1}^N \sum_{\alpha, \beta=1}^4 w_{i\alpha} (\tilde{\tau}_x \tilde{\sigma}_y)_{\alpha, \beta} w_{i\beta} + \Delta \sum_{i=1}^N \sum_{\alpha, \beta=1}^4 w_{i\alpha} (\tilde{\tau}_y \tilde{\sigma}_x)_{\alpha, \beta} w_{i\beta} + \frac{i\gamma}{2} \sum_{i=1}^N \sum_{\alpha, \beta=1}^4 w_{i\alpha} (\tilde{\tau}_0 \tilde{\sigma}_0 + \tilde{\tau}_x \tilde{\sigma}_0)_{\alpha, \beta} w_{i\beta} + \text{H.c.}, \quad (9a)$$

$$X_1 = \mu_1 \sum_{i=1}^N \sum_{\alpha, \beta=1}^4 w_{i\alpha} (\tilde{\tau}_0 \tilde{\sigma}_y)_{\alpha, \beta} w_{i\beta} + \frac{i\gamma}{2} \sum_{i=1}^N \sum_{\alpha, \beta=1}^4 w_{i\alpha} (\tilde{\tau}_0 \tilde{\sigma}_0 + \tilde{\tau}_x \tilde{\sigma}_0)_{\alpha, \beta} w_{i\beta}. \quad (9b)$$

Here,  $\tilde{\tau}$  and  $\tilde{\sigma}$  denote Pauli matrices representing the dressed degrees of freedom as compared to the original degrees of freedom. Therefore, the Floquet damping matrix  $X_F$  can be constructed as

$$U_X(T, 0) \equiv e^{iX_F T} = e^{iX_1 \frac{T}{4}} e^{iX_0 \frac{T}{2}} e^{iX_1 \frac{T}{4}}. \quad (10)$$

Here,  $U_X(T, 0)$  is a time-evolution operator involving only the Floquet damping matrices. We extract the quasienergy  $E_{n,k}$  from the eigenvalue equation:  $e^{iX_F T} |\psi_n\rangle = \exp(iE_n T) |\psi_n\rangle$ , where the quasienergy  $E_n$  is now a complex number.

#### IV. TOPOLOGICAL CHARACTERIZATION

To extract the topological invariant from  $X_F$ , we rely on the pseudo-anti-Hermitian symmetry  $\Gamma = \tilde{\tau}_x \tilde{\sigma}_x$ . This symmetry  $\Gamma$  is also called the generalized chiral symmetry for an NH Hamiltonian [92]. Both the step damping matrices  $X_0$  [Eq. (9a)] and  $X_1$  [Eq. (9b)] satisfies this symmetry, such that  $\Gamma X_i \Gamma = -X_i^\dagger$ ; with  $i = 0, 1$ . The operator  $U_X(T, 0)$  under the pseudo-anti-Hermitian symmetry transforms as  $\Gamma U_X(T, 0) \Gamma = U_X^\dagger(T, 0)$ . We provide this proof in Appendix A. Additionally, the pseudo-anti-Hermitian symmetry divides the full time period into two parts such that: First part  $U_c = U_X(T/2, 0)$  and second part  $\Gamma U_c^\dagger \Gamma = U_X(T, T/2)$  [93]. Using these two parts, we can define two operators:  $U_X^\dagger = \Gamma U_c^\dagger \Gamma U_c$  and  $U_X = U_c \Gamma U_c^\dagger \Gamma$ . The operators  $U_X^{1,2}$  satisfies  $\Gamma U_X^{1,2}(T, 0) \Gamma = U_X^{1,2\dagger}(T, 0)$ . Accordingly, we can define two Floquet damping matrices as  $X_F^{1,2} = \frac{i}{T} \ln U_X^{1,2}$  with  $X_F^{1,2}$  satisfying the pseudo-anti-Hermitian symmetry:  $\Gamma X_F^{1,2} \Gamma = -X_F^{1,2\dagger}$ . The pseudo-anti-Hermitian symmetry demands the left and right eigenstates ( $|\psi_{L,n}^{1,2}\rangle$  and  $|\psi_{R,n}^{1,2}\rangle$ ) and the eigen-

values  $E_n^{1,2}$  of  $X_F^{1,2}$  to satisfy:  $|\psi_{L,n}^{1,2}\rangle = \Gamma |\psi_{R,n}^{1,2}\rangle$  and  $E_{-n}^{1,2*} = -E_n^{1,2}$  [94]. Using these properties, we can construct an operator  $Q^{1,2}$  as

$$Q^{1,2} = \frac{1}{2} \left( \sum_{n>0} |\psi_{L,n}^{1,2}\rangle \langle \psi_{R,n}^{1,2}| - \sum_{n<0} |\psi_{L,n}^{1,2}\rangle \langle \psi_{R,n}^{1,2}| \right. \\ \left. + \sum_{n>0} |\psi_{R,n}^{1,2}\rangle \langle \psi_{L,n}^{1,2}| - \sum_{n<0} |\psi_{R,n}^{1,2}\rangle \langle \psi_{L,n}^{1,2}| \right). \quad (11)$$

Here,  $Q^{1,2}$  is a Hermitian matrix and satisfies  $\Gamma Q^{1,2} \Gamma = -Q^{1,2}$ , such that  $\Gamma$  is an effective chiral symmetry for  $Q^{1,2}$ . Now, we employ the basis in which  $\Gamma$  is diagonal such that  $U_\Gamma \Gamma U_\Gamma^{-1} = \text{diag}(1, \dots, 1, -1, \dots, -1)$ . In this basis, the matrix  $Q^{1,2}$  takes a block anti-diagonal form

$$U_\Gamma Q^{1,2} U_\Gamma^{-1} = \begin{pmatrix} 0 & q^{1,2} \\ q^{1,2\dagger} & 0 \end{pmatrix}. \quad (12)$$

Also, the +1 and -1 eigenvalues effectively provide us with two sublattice degrees of freedom  $A$  and  $B$ , respectively. We can represent  $\Gamma$  as  $\Gamma = U_A^\Gamma - U_B^\Gamma$ ; with  $U_A^\Gamma = \sum |A\rangle \langle A|$  and  $U_B^\Gamma = \sum |B\rangle \langle B|$ . Now, we perform a singular value decomposition of  $q^{1,2}$  as  $q^{1,2} = U_A^{1,2} \Sigma^{1,2} U_B^{1,2\dagger}$ , with  $U_{A,B}^{1,2}$  and  $\Sigma^{1,2}$  containing the singular vectors and singular values, respectively. Using  $U_{A,B}^{1,2}$  and  $U_{A,B}^{1,2}$ , we define the winding numbers  $\nu_{1,2}$  associated to the Floquet damping matrices  $X_F^{1,2}$  as [95]

$$\nu_{1,2} = \frac{1}{2\pi i} \text{Tr} [\ln (\bar{P}_A^{1,2} \bar{P}_B^{1,2\dagger})], \quad (13)$$

where the sublattice dipole moment operators  $\bar{P}_A^{1,2}$  and  $\bar{P}_B^{1,2}$  are restricted to the sublattice  $A$  and  $B$ , respectively. Explicitly,  $\bar{P}_{A,B}^{1,2}$  are defined as  $\bar{P}_{A,B}^{1,2} =$



$U_{A,B}^{1,2\dagger} U_{A,B}^{\Gamma\dagger} P U_{A,B}^{\Gamma} U_{A,B}^{1,2}$  with the dipole moment operator  $P = \exp(-2\pi i x/N)$ . Finally, we combine  $\nu_{1,2}$  in such a way that the number of 0-modes  $2\nu_0$  and  $\pi$ -modes  $2\nu_\pi$  are given as [93]

$$\nu_0 = \frac{\nu_1 + \nu_2}{2}, \quad \text{and} \quad \nu_\pi = \frac{\nu_1 - \nu_2}{2}. \quad (14)$$

We use  $\nu_{0,\pi}$  to topologically characterize the 0- and  $\pi$ -modes that emerges in our system.

## V. RESULTS

In this section, we discuss the numerical results associated with the driven-dissipative Rashba nanowire. First, we show the emergence of the MZMs and MPMs using the Floquet damping matrix. Note that we always use a finite system obeying open boundary condition (OBC) while discussing the spectral properties: Eigenvalue spectra and local density of states (LDOS). To compute the winding numbers, we consider periodic boundary condition (PBC). We also discuss the TZMs and TPMs and link their emergence to the EPs. Then we study the topological phase diagrams of this driven-dissipative system.

### A. Emergence of MZMs and MPMs

First, we demonstrate the generation of the MZMs and MPMs. We investigate the quasienergy spectra  $E$  of the Floquet damping matrix  $X_F$  as a function of  $B$  in Fig. 1(a) for a system obeying OBC. The quasienergy  $E$  is a complex number in the presence of dissipation, and we show the real part of the quasienergy spectra  $\text{Re } E$  while the imaginary part  $\text{Im } E$  is represented by the colormap in Fig. 1(a). The quasienergy spectra reveal the appearance of states near quasienergy  $\text{Re } E = 0, \pm\pi$ . There are two different kinds of states that appear at these quasienergies, and we distinguish them in the forthcoming text. However, these modes at  $\text{Re } E = 0, \pm\pi$  also acquire a finite imaginary part in the dissipative background, implying their state would decay with time.

In Fig. 1(a), the regions marked by yellow host modes are either at quasienergy 0 or  $\pm\pi$ , which we refer to as TZM and TPMs, respectively, that are not connected to the bulk topology of the system. The driven system further hosts MZMs and MPMs that are connected to the bulk topology of the system. The Majorana modes appearing at quasienergy  $\text{Re } E = \pm\pi$  are unique to a driven system and have no static analog. Moreover, the driven system also supports MZMs for a magnetic field  $B$  that is less than a static system's critical field, thereby extending the topological phase boundaries.

To verify that the MZMs and MPMs (TZMs and TPMs) are (not) directly linked to bulk gap closing and reopening, we also study the quasienergy spectra employing the PBC [red dots] and compare them with the OBC

[gray dots] spectra in Figs. 1(b) and (c), respectively. Note that we have verified that our system is free from the NH skin effect, owing to the particular form of the loss operator in Eq. (5). Thus, the gap-closing points in PBC spectra coincide with those of OBC, indicating the topological phase boundaries. First, we focus on the modes that appear at quasienergy 0 in Fig. 1(b) (we show the  $\text{Re } E$  close to zero). Figure 1(b) shows some modes appear at  $\text{Re } E = 0$  in the OBC spectra, but these modes are not directly connected to bulk gap closing-reopening from one side in the PBC spectra. These modes are denoted as TZMs, and we mark regions with TZMs with yellow shades. The TZMs are connected to the EPs that we discuss in detail in the subsequent text. However, importantly, there also exist Majorana modes that appear at  $\text{Re } E = 0$  with connection to bulk gap closing-opening.

To further verify our claim that the MZMs (TZMs) are topologically non-trivial (trivial), we compute the winding number  $\nu_0$  and show the same by the solid blue line in Fig. 1(b). The non-zero values of  $\nu_0 = 1$  coincide with regions with MZMs. Also,  $\nu_0$  shows a transition from 1 (topological) to 0 (trivial) via bulk gap closing. Similarly, we also distinguish between the MPMs and TPMs by investigating the quasienergy spectra in PBC (red dots) and OBC (gray dots) close to  $\text{Re } E = \pi$  in Fig. 1(c). Note that in this case, the eigenvalue spectra touching at  $\text{Re } E = \pi$  imply a gap closing at that energy. The TPMs are not directly connected to bulk gap closing-reopening from one side at  $\text{Re } E = \pi$ , but are rather connected to the EPs, which are discussed below. The regions with TPMs are shaded in yellow. On the other hand, the MPMs appear with a bulk gap closing and also carry a non-zero winding number  $\nu_\pi = 1, 2$ , see the blue solid line in Fig. 1(c). Together in Figs. 1(a-c), we establish that the driven-dissipative system hosts topologically non-trivial (trivial) MZMs and MPMs (TZMs and TPMs).

Now, we tie the emergence of the TZMs and TPMs to the EPs that appear in the spectra [82]. Although one side of the yellow regions in Figs. 1(a-c), which indicates the TZMs and TPMs, represents bulk gap closing, the appearance and disappearance of these modes are not directly linked to the bulk gap opening and reopening. Here, we discuss how the EPs play a crucial role in the emergence and destruction of the TZMs and TPMs. First, we consider the TZMs and focus on the regions that appear close to  $B = 4$  in Fig. 1(b). The left side of this yellow region is a bulk gap closing point. However, the TZMs in this region can be destroyed without closing any bulk gap as happens at the point indicated by the black dashed line in Fig. 1(b) [ $B \simeq 4.473$ ]. Focusing on this particular value of the magnetic field  $B$ , we show the formation of two second-order EPs in Fig. 1(d): the  $(2N-1)$ -th (blue) state coalesce with  $(2N+1)$ -th (orange) state and  $E_{2N}$ -th (black) state coalesce with  $(2N+2)$ -th (green) state and, thus, forms two second-order EPs. At this point, the real, imaginary, and absolute eigenvalues of these states become degenerate. In Fig. 1(d), we only show the absolute eigenvalue  $|E|$  as a function of  $B$ , but

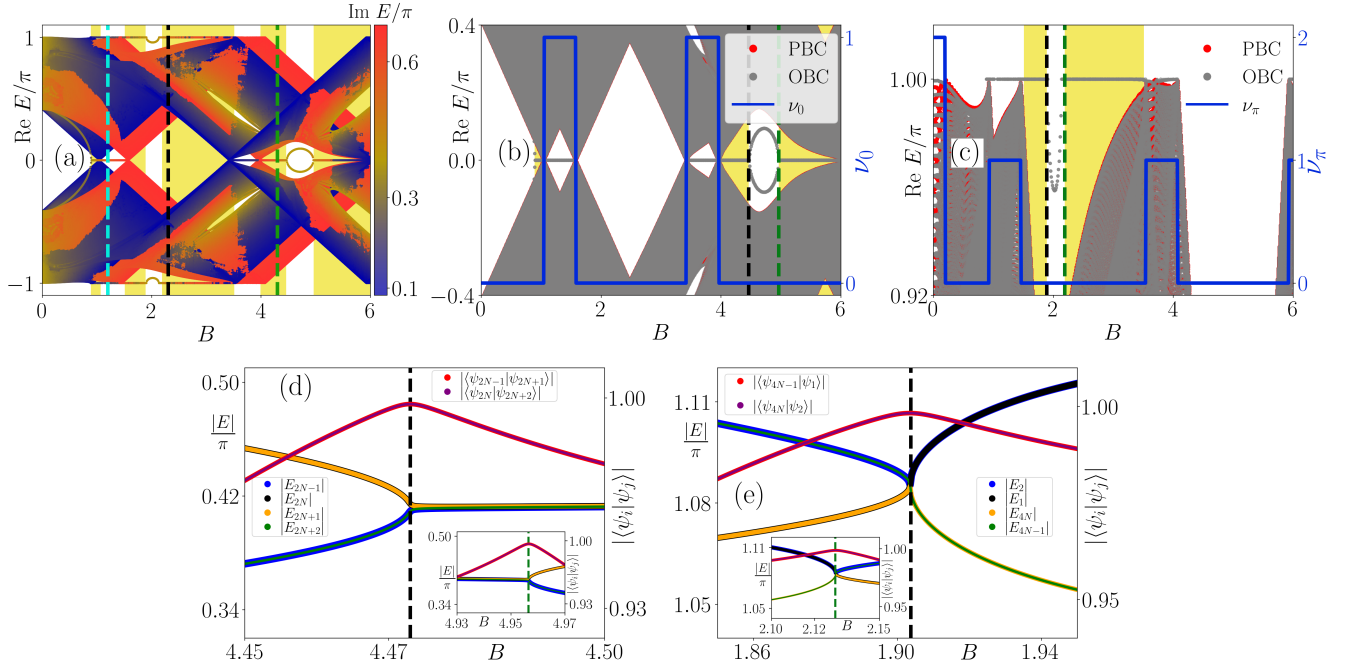


FIG. 1. (a) Real part of the quasienergy  $\text{Re } E$  as a function of the magnetic field  $B$  of the Floquet damping matrix, considering OBC. The color represents the imaginary part of the quasienergy  $\text{Im } E$  and the amplitude is represented by the colorbar. The cyan, black, and green dashed lines represent parameters used in Fig. 2. The yellow shade represents regions of TZMs and TPMS. We use 100 lattice sites. (b) Quasienergy spectra close to  $\text{Re } E = 0$  for a system obeying PBC (red) and OBC (gray). The right axis represents the winding number  $\nu_0$ . We use 400 lattice sites. (c) We repeat (b) but close to  $\text{Re } E = \pi$  and the right axis represent the winding number  $\nu_\pi$ . (d) The absolute quasienergy  $|E|$  as a function of  $B$  is shown close to the black dashed line in (b). The right axis represents the scalar product  $|\langle \psi_i | \psi_j \rangle|$ . The inset shows  $|E|$  and  $|\langle \psi_i | \psi_j \rangle|$  close to the green dashed line in (b). (e) We repeat (d) but for the black and green dashed lines in (c). Here,  $2t_h = \lambda_R = \Delta = \gamma = 1$ ,  $\mu = 0$ ,  $\mu_1 = 0.3$ , and  $\omega = 2.5$ .

the real and imaginary parts also show a similar behavior. Note that we sort the eigenvalues using the real part of the eigenvalues.

We also investigate the scalar product between these eigenstates in the right axis of Fig. 1(d). Moreover, the scalar product of the eigenstates  $|\langle \psi_{2N-1} | \psi_{2N+1} \rangle|$  (red) and  $|\langle \psi_{2N} | \psi_{2N+2} \rangle|$  (purple) also becomes unity, indicating that these states become pairwise parallel to each other. Thus, the black dashed line in Fig. 1(b) indicates EPs, and the formation of EPs destroys the TZMs. On the other hand, the TZMs can also be created by forming EPs, which happens at the green dashed line in Fig. 1(b). At this point, we see the formation of two second-order EPs, which are shown in the inset of Fig. 1(d). In the literature, the EPs have been shown to have a topological nature and can be connected to energy-based topological indices [43, 44, 47–53]. Here, we demonstrate that the EPs can also create and destroy trivial edge modes.

Furthermore, we also relate the emergence and destruction of TPMS to the EPs. Note that the yellow shaded region is bounded by EP and bulk gap closing. In this regard, we focus on the black and green dashed line in Fig. 1(c), which indicates the destruction and emergence of the TPMS. Focusing on these lines, we show the formation of two second-order EPs as a function of  $B$  in

Fig. 1(e). The  $(4N - 1)$ -th (green) state coalesces with the 1-st (black) state, and the  $4N$ -th (orange) state coalesces with the 2-nd (blue) state, forming two second-order EPs. Note that the 1-st and 2-nd eigenstates appear at quasienergy  $-\pi$ , but in a Floquet system, the quasienergy  $-\pi$  is equivalent to quasienergy  $+\pi$ . The scalar product of the eigenstates (shown on the right axis of Fig. 1(e))  $|\langle \psi_{4N-1} | \psi_1 \rangle|$  (red) and  $|\langle \psi_{4N} | \psi_2 \rangle|$  (purple) also becomes unity, indicating that these states become pairwise parallel to each other. Thus, the black dashed line in Fig. 1(c) indicates EPs. Similarly, at the green dashed line in Fig. 1(c), we also obtain two second-order EPs, and their formation is shown in the inset of Fig. 1(e). In summary, the EPs play a key role in the formation of the TZMs and TPMS in a driven system, demonstrating its significance in shaping the system's dynamics and spectral properties. Our observation is not limited by any specific choice of parameters and is a property of the driven Rashba nanowire in the presence of the dissipation of the form given in Eq. (5).

Having discussed the emergence of different kinds of 0 and  $\pi$ -modes in the system, we now demonstrate their localization properties in Fig. 2. To this end, we focus on some specific parameters as indicated by the cyan, black, and green lines in Fig. 1(a). For the cyan line in

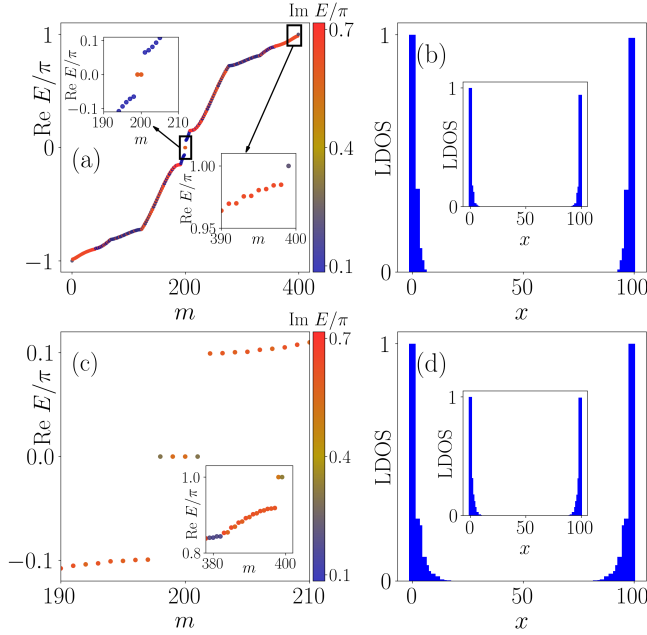


FIG. 2. (a) Real part of the quasienergy spectrum  $\text{Re } E$  as a function of  $m$  for  $B = 1.2$  (cyan line in Fig. 1(a)). The insets represent zoomed-in spectra close to  $\text{Re } E = 0$  and  $\pi$ . The color bar indicates the imaginary part of the quasienergy. (b) LDOS associated with the MZMs, while the inset shows the LDOS for the MPMs. (c) Real part of the quasienergy spectrum close to  $\text{Re } E = 0.0$  showing four TZMs for  $B = 4.3$  (green line in Fig. 1(a)). The inset shows real part of the quasienergy spectrum close to  $\text{Re } E = \pi$ , showing two TPMs (the other two appear at  $\text{Re } E = -\pi$ ) for  $B = 2.3$  (black line in Fig. 1(a)). (d) LDOS associated with the TZMs. The inset shows the LDOS for the TPMs. We consider  $N = 100$  lattice sites and the rest of the parameters remain the same as in Fig. 1.

Fig. 1(a), we show the real part of eigenvalue spectrum  $\text{Re } E$  of the Floquet damping matrix  $X_F$  obeying OBC as a function of the eigenvalue index  $m$  in Fig. 2(a). The color bar represents the imaginary part of the eigenvalue  $\text{Im } E$ . In the insets, we show zoomed-in spectra close to  $\text{Re } E = 0$  and  $\text{Re } E = \pi$ , which exhibit the presence of two MZMs and MPMs, respectively. Note that for this parameter, the system also exhibits a non-zero winding number  $\nu_{0,\pi} = 1$ . On the other hand, both the MZMs and MPMs have a non-zero imaginary part, as seen from the color of the eigenvalues. Thus, the MZMs and MPMs have a finite lifetime. We compute the local density at  $\text{Re } E = 0$  and  $\pm\pi$  and show them in Fig. 2(b) and its inset, respectively, which show the edge localization of the Majorana modes.

To focus on the TZMs and TPMs, we now consider the green and black lines in Fig. 1(a). For the green (black) line, the system exhibits four modes at quasienergy  $\text{Re } E = 0$  (two modes each at quasienergy  $\text{Re } E = +\pi$  and  $-\pi$ ), which is demonstrated in Fig. 2(c) (inset of Fig. 2(c)). These modes, however, do not carry any wind-

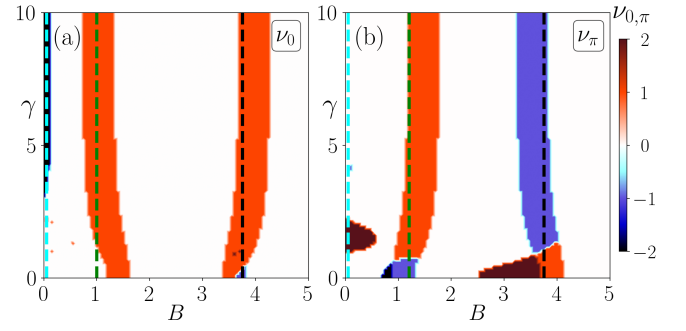


FIG. 3. The Phase diagram in terms of (a)  $\nu_0$  and (b)  $\nu_\pi$  in the  $B$ - $\gamma$  plane. The  $\gamma = 0$  line represents the Hermitian driven system. Here, the colorbar represents the values of  $\nu_{0,\pi}$ . We consider 200 lattice sites. Rest of the parameters remain the same as in Fig. 1.

ing number i.e.,  $\nu_{0,\pi} = 0$ . Hence, they are denoted as TZMs and TPMs. Nevertheless, the TZMs and TPMs are also located at the edges of the system, as shown in Fig. 2(d) and its inset, respectively. Note that our system is free from the NH skin-effect; thus, the boundary modes that appear in our system are either MZMs, MPMs, TZMs, or TPMs.

In this subsection, we demonstrate that the drive-dissipative system hosts topologically non-trivial MZMs and MPMs, which are topologically characterized by non-zero winding numbers. The interplay of dissipation and periodic drive also gives rise to trivial boundary modes both at quasienergy 0 and  $\pi$ , which are not connected to any bulk topology; rather, their creation and destruction are linked to the EPs. The MPMs and TPMs only appear in a driven-dissipative system and have no static analog [82].

## B. Phase diagram and higher winding numbers

Having discussed the spectral properties of the system, we now investigate the phase diagram of this driven-dissipative system in Fig. 3. In particular, we show the winding number  $\nu_0$  and  $\nu_\pi$  in the  $B$ - $\gamma$  plane in Figs. 3(a) and (b), respectively. Focusing on  $\nu_0$  in Fig. 3(a), we observe phases with winding numbers  $\nu_0 \geq \pm 1$ , which indicates the appearance of multiple (more than two) edge-localized MZMs. Generation of multiple topological modes is one of the salient features of the driven system [33]. Furthermore, if we compare the  $\nu_0$  between  $\gamma = 0$  (Hermitian case) and  $\gamma > 0$  (non-Hermitian case), we observe a phase transition with respect to  $\gamma$ . To further elucidate this, we draw a few vertical lines in Fig. 3(a): cyan ( $B = 0.05$ ), green ( $B = 1.0$ ), and black ( $B = 3.75$ ). The cyan and green lines indicate a phase transition as a function of  $\gamma$  for a magnetic field  $B < B_{c1} (= \sqrt{2})$ . Thus, in a driven-dissipative system, we can obtain the MZMs for a lesser strength of applied magnetic field compared to the static system, which can be

advantageous for an experimental setup. Furthermore, the black dashed line reveals a change in winding number  $\nu_0 = -1 \rightarrow 1$  as a function of the dissipation strength  $\gamma$ . Thus, the phase diagram Fig. 3(a) indicates that the dissipation can substantially modify the topological phases of the driven system and induce topological states which are only realized in the presence of dissipation [82]. This is one of the key observations of this work.

We also obtain a rich phase diagram for the MPMs, see Fig. 3(b), where we show  $\nu_\pi$  in the  $B$ - $\gamma$  plane. As mentioned before, the generation of the MPMs is unique to a driven system without any static analog. Figure 3(b) exhibits phases with a higher winding number  $\nu_\pi > \pm 1$ , which indicates generation of multiple MPMs [33]. Moreover, Fig. 3(b) suggests the topological phase transition with respect to  $\gamma$ , and also, there are some phases that do not exist in the closed driven system, i.e., the Hermitian case. To investigate this further, we draw a few vertical lines: cyan ( $B = 0.5$ ), green ( $B = 1.2$ ), and black ( $B = 3.75$ ). These lines demonstrate the change in winding number  $\nu_\pi$  as a function of  $\gamma$  and show how dissipation changes the topology of the system compared to a Hermitian-driven system. Together in Fig. 3, we uncover the important role of dissipation in shaping the topological phases in a driven system.

## VI. SUMMARY AND DISCUSSION

In this work, we consider a Rashba nanowire in close proximity to an  $s$ -wave superconductor. We use a periodic step-drive and assume an onsite loss in the system. The dynamics of the system is governed by a periodic Lindbladian. We employ the third-quantization method to obtain the Floquet Lindbladian and thereby the Floquet damping matrix that provides the spectral and topological properties of the system. Our system is free from skin-effect for this choice of jump operator. We investigate the spectra of the Floquet damping matrix and show the existence of the MZMs and MPMs. The MZMs and MPMs, however, get a finite imaginary part in the presence of dissipation. Additionally, the driven-dissipative system also hosts TZMs and TPMs, whose origin is not connected to the bulk topology of the system; rather, they are induced by the EPs. We compute the topological invariant based on pseudo-anti-Hermitian symmetry to show that the MZMs and MPMs are indeed topological. We also study the localization properties of the MZMs, MPMs, TZMs, and TPMs, and establish their edge localization. Furthermore, we utilize the topological invariant to obtain a phase diagram for this driven-dissipative system. The phase diagram suggests that the dissipation plays an important role in shaping the topological nature of the system and even induces topological

phases in the system that are absent in the closed driven system.

In this work, we only consider a 1D Rashba nanowire. However, the MZMs and MPMs can also appear in higher dimensions, such as the corner modes of a two-dimensional second-order topological superconductor (SOTSC) and a three-dimensional third-order topological superconductor (TOTSC) [32]. Thus, one of the interesting outlooks can be to investigate the effect of dissipation in a driven SOTSC and TOTSC and see if the dissipation can induce the MZMs and MPMs in these systems. Also, it would be fascinating to explore if one can also obtain the TZMs and TPMs as the corner modes in these systems.

## Data Availability

The data that support the findings of this article are openly available at Ref. [96].

## ACKNOWLEDGMENTS

K.G. and T.N. acknowledge the NFSG “NFSG/HYD/2023/H0911” from BITS Pilani.

## Appendix A: $U_X(T, 0)$ under chiral symmetry

Here, we discuss how the operator  $U_X(t, 0)$  transforms under pseudo-anti-Hermitian symmetry  $\Gamma$ . The damping matrix  $X(t)$  transforms under pseudo-anti-Hermitian symmetry as  $\Gamma X(t)\Gamma = -X^\dagger(T-t)$ . Employing this property, we can obtain the effect on  $U_X(t, 0)$  as

$$\begin{aligned} \Gamma U_X(t, 0) \Gamma &= \Gamma \left[ \text{TO} \exp \left( -i \int_0^t X(t') dt' \right) \right] \Gamma \\ &= \sum_m \frac{(-i)^m}{m!} \text{TO} \int_0^t dt'_1 \dots \int_0^t dt'_m \Gamma X(t'_1) \Gamma \dots \Gamma X(t'_m) \Gamma \\ &= \sum_m \frac{(i)^m}{m!} \text{TO} \int_0^t dt'_1 \dots \int_0^t dt'_m X^\dagger(T-t'_1) \dots X^\dagger(T-t'_m) \\ &= \sum_m \frac{(-i)^m}{m!} \text{TO} \int_T^{T-t} dt'_1 \dots \int_T^{T-t} dt'_m X^\dagger(t'_1) \dots X^\dagger(t'_m) \\ &= \text{TO} \exp \left( -i \int_T^{T-t} X^\dagger(t') dt' \right). \end{aligned} \quad (\text{A1})$$

Thus, at the full time-period  $T$ , the operator  $U_X(T, 0)$  transforms  $\Gamma U_X(T, 0) \Gamma = \text{TO} \exp \left( -i \int_T^0 X^\dagger(t') dt' \right) \equiv U_X^\dagger(T, 0)$ .

[1] A. Y. Kitaev, “Unpaired Majorana fermions in quantum wires,” *Phys.-Usp.* **44**, 131 (2001).

[2] X.-L. Qi and S.-C. Zhang, “Topological insulators and superconductors,” *Rev. Mod. Phys.* **83**, 1057 (2011).



- [3] M. Leijnse and K. Flensberg, “Introduction to topological superconductivity and Majorana fermions,” *Semicond. Sci. Technol.* **27**, 124003 (2012).
- [4] J. Alicea, “New directions in the pursuit of Majorana fermions in solid state systems,” *Rep. Prog. Phys.* **75**, 076501 (2012).
- [5] C. Beenakker, “Search for Majorana fermions in superconductors,” *Annu. Rev. Condens. Matter Phys.* **4**, 113 (2013).
- [6] R. Aguado, “Majorana quasiparticles in condensed matter,” *Riv. Nuovo Cimento* **40**, 523 (2017).
- [7] Y. Tanaka, S. Tamura, and J. Cayao, “Theory of majorana zero modes in unconventional superconductors,” *Prog. Theor. Exp. Phys.*, ptae065 (2024).
- [8] Y. Oreg, G. Refael, and F. von Oppen, “Helical Liquids and Majorana Bound States in Quantum Wires,” *Phys. Rev. Lett.* **105**, 177002 (2010).
- [9] R. M. Lutchyn, J. D. Sau, and S. Das Sarma, “Majorana Fermions and a Topological Phase Transition in Semiconductor-Superconductor Heterostructures,” *Phys. Rev. Lett.* **105**, 077001 (2010).
- [10] V. Mourik, K. Zuo, S. M. Frolov, S. R. Plissard, E. P. A. M. Bakkers, and L. P. Kouwenhoven, “Signatures of Majorana Fermions in Hybrid Superconductor-Semiconductor Nanowire Devices,” *Science* **336**, 1003 (2012).
- [11] A. Das, Y. Ronen, Y. Most, Y. Oreg, M. Heiblum, and H. Shtrikman, “Zero-bias peaks and splitting in an Al-InAs nanowire topological superconductor as a signature of Majorana fermions,” *Nature Phys* **8**, 887 (2012).
- [12] M. T. Deng, C. L. Yu, G. Y. Huang, M. Larsson, P. Caroff, and H. Q. Xu, “Anomalous Zero-Bias Conductance Peak in a Nb-InSb Nanowire-Nb Hybrid Device,” *Nano Lett.* **12**, 6414 (2012), pMID: 23181691.
- [13] L. P. Rokhinson, X. Liu, and J. K. Furdyna, “The fractional a.c. Josephson effect in a semiconductor-superconductor nanowire as a signature of Majorana particles,” *Nature Phys* **8**, 795 (2012).
- [14] A. D. K. Finck, D. J. Van Harlingen, P. K. Mohseni, K. Jung, and X. Li, “Anomalous Modulation of a Zero-Bias Peak in a Hybrid Nanowire-Superconductor Device,” *Phys. Rev. Lett.* **110**, 126406 (2013).
- [15] S. M. Albrecht, A. P. Higginbotham, M. Madsen, F. Kuemmeth, T. S. Jespersen, J. Nygård, P. Krogstrup, and C. M. Marcus, “Exponential protection of zero modes in Majorana islands,” *Nature* **531**, 206 (2016).
- [16] M. T. Deng, S. Vaitiekenas, E. B. Hansen, J. Danon, M. Leijnse, K. Flensberg, J. Nygård, P. Krogstrup, and C. M. Marcus, “Majorana bound state in a coupled quantum-dot hybrid-nanowire system,” *Science* **354**, 1557 (2016).
- [17] F. Nichele, A. C. C. Drachmann, A. M. Whiticar, E. C. T. O’Farrell, H. J. Suominen, A. Fornieri, T. Wang, G. C. Gardner, C. Thomas, A. T. Hatke, P. Krogstrup, M. J. Manfra, K. Flensberg, and C. M. Marcus, “Scaling of Majorana Zero-Bias Conductance Peaks,” *Phys. Rev. Lett.* **119**, 136803 (2017).
- [18] J. Chen, P. Yu, J. Stenger, M. Hoeschele, D. Car, S. R. Plissard, E. P. A. M. Bakkers, T. D. Stanescu, and S. M. Frolov, “Experimental phase diagram of zero-bias conductance peaks in superconductor/semiconductor nanowire devices,” *Sci. Adv.* **3**, e1701476 (2017).
- [19] H. Zhang, Ö. Gül, S. Conesa-Boj, M. P. Nowak, M. Wimmer, K. Zuo, V. Mourik, F. K. de Vries, J. van Veen, M. W. A. de Moor, J. D. S. Bommer, D. J. van Woerkom, D. Car, S. R. Plissard, E. P. Bakkers, M. Quintero-Pérez, M. C. Cassidy, S. Koelling, S. Goswami, K. Watanabe, T. Taniguchi, and L. P. Kouwenhoven, “Ballistic superconductivity in semiconductor nanowires,” *Nat Commun* **8**, 16025 (2017).
- [20] Ö. Gül, H. Zhang, J. D. S. Bommer, M. W. A. de Moor, D. Car, S. R. Plissard, E. P. A. M. Bakkers, A. Geresdi, K. Watanabe, T. Taniguchi, and L. P. Kouwenhoven, “Ballistic Majorana nanowire devices,” *Nature Nanotech* **13**, 192 (2018).
- [21] A. Grivnin, E. Bor, M. Heiblum, Y. Oreg, and H. Shtrikman, “Concomitant opening of a bulk-gap with an emerging possible Majorana zero mode,” *Nat Commun* **10**, 1940 (2019).
- [22] J. Chen, B. D. Woods, P. Yu, M. Hoeschele, D. Car, S. R. Plissard, E. P. A. M. Bakkers, T. D. Stanescu, and S. M. Frolov, “Ubiquitous Non-Majorana Zero-Bias Conductance Peaks in Nanowire Devices,” *Phys. Rev. Lett.* **123**, 107703 (2019).
- [23] M. Leijnse and K. Flensberg, “Parity qubits and poor man’s Majorana bound states in double quantum dots,” *Phys. Rev. B* **86**, 134528 (2012).
- [24] T. Dvir, G. Wang, N. van Loo, C.-X. Liu, G. P. Mazur, A. Bordin, S. L. D. ten Haaf, J.-Y. Wang, D. van Driel, F. Zatelli, X. Li, F. K. Malinowski, S. Gazibegovic, G. Badawy, E. P. A. M. Bakkers, M. Wimmer, and L. P. Kouwenhoven, “Realization of a minimal Kitaev chain in coupled quantum dots,” *Nature* **614**, 445 (2023).
- [25] L. Jiang, T. Kitagawa, J. Alicea, A. R. Akhmerov, D. Pekker, G. Refael, J. I. Cirac, E. Demler, M. D. Lukin, and P. Zoller, “Majorana Fermions in Equilibrium and in Driven Cold-Atom Quantum Wires,” *Phys. Rev. Lett.* **106**, 220402 (2011).
- [26] M. Thakurathi, A. A. Patel, D. Sen, and A. Dutta, “Floquet generation of Majorana end modes and topological invariants,” *Phys. Rev. B* **88**, 155133 (2013).
- [27] D. E. Liu, A. Levchenko, and H. U. Baranger, “Floquet Majorana Fermions for Topological Qubits in Superconducting Devices and Cold-Atom Systems,” *Phys. Rev. Lett.* **111**, 047002 (2013).
- [28] M. Benito, A. Gómez-León, V. M. Bastidas, T. Brandes, and G. Platero, “Floquet engineering of long-range p-wave superconductivity,” *Phys. Rev. B* **90**, 205127 (2014).
- [29] A. C. Potter, T. Morimoto, and A. Vishwanath, “Classification of Interacting Topological Floquet Phases in One Dimension,” *Phys. Rev. X* **6**, 041001 (2016).
- [30] M. Thakurathi, D. Loss, and J. Klinovaja, “Floquet Majorana fermions and parafermions in driven Rashba nanowires,” *Phys. Rev. B* **95**, 155407 (2017).
- [31] Z. Yang, Q. Yang, J. Hu, and D. E. Liu, “Dissipative Floquet Majorana Modes in Proximity-Induced Topological Superconductors,” *Phys. Rev. Lett.* **126**, 086801 (2021).
- [32] A. K. Ghosh, T. Nag, and A. Saha, “Dynamical construction of quadrupolar and octupolar topological superconductors,” *Phys. Rev. B* **105**, 155406 (2022).
- [33] D. Mondal, A. K. Ghosh, T. Nag, and A. Saha, “Topological characterization and stability of Floquet Majorana modes in Rashba nanowires,” *Phys. Rev. B* **107**, 035427 (2023).

- [34] D. Mondal, A. K. Ghosh, T. Nag, and A. Saha, “Engineering anomalous Floquet Majorana modes and their time evolution in a helical Shiba chain,” *Phys. Rev. B* **108**, L081403 (2023).
- [35] A. K. Ghosh, T. Nag, and A. Saha, “Time evolution of Majorana corner modes in a Floquet second-order topological superconductor,” *Phys. Rev. B* **107**, 035419 (2023).
- [36] K. Roy and S. Basu, “Single and multifrequency driving protocols in a Rashba nanowire proximitized to an s-wave superconductor,” *Phys. Rev. B* **110**, 165403 (2024).
- [37] R. W. Bomantara and J. Gong, “Quantum computation via Floquet topological edge modes,” *Phys. Rev. B* **98**, 165421 (2018).
- [38] B. Bauer, T. Pereg-Barnea, T. Karzig, M.-T. Rieder, G. Refael, E. Berg, and Y. Oreg, “Topologically protected braiding in a single wire using Floquet Majorana modes,” *Phys. Rev. B* **100**, 041102 (2019).
- [39] L. Zhou, “Non-Hermitian Floquet topological superconductors with multiple Majorana edge modes,” *Phys. Rev. B* **101**, 014306 (2020).
- [40] A. K. Ghosh and T. Nag, “Non-Hermitian higher-order topological superconductors in two dimensions: Statics and dynamics,” *Phys. Rev. B* **106**, L140303 (2022).
- [41] S. Yao and Z. Wang, “Edge States and Topological Invariants of Non-Hermitian Systems,” *Phys. Rev. Lett.* **121**, 086803 (2018).
- [42] F. K. Kunst, E. Edvardsson, J. C. Budich, and E. J. Bergholtz, “Biorthogonal Bulk-Boundary Correspondence in Non-Hermitian Systems,” *Phys. Rev. Lett.* **121**, 026808 (2018).
- [43] E. J. Bergholtz, J. C. Budich, and F. K. Kunst, “Exceptional topology of non-Hermitian systems,” *Rev. Mod. Phys.* **93**, 015005 (2021).
- [44] N. Okuma and M. Sato, “Non-Hermitian Topological Phenomena: A Review,” *Annu. Rev. Condens. Matter Phys.* **14**, 83 (2023).
- [45] C. H. Lee and R. Thomale, “Anatomy of skin modes and topology in non-Hermitian systems,” *Phys. Rev. B* **99**, 201103 (2019).
- [46] L. Li, C. H. Lee, S. Mu, and J. Gong, “Critical non-Hermitian skin effect,” *Nat Commun* **11**, 5491 (2020).
- [47] A. Banerjee, R. Sarkar, S. Dey, and A. Narayan, “Non-Hermitian topological phases: principles and prospects,” *J. Phys.: Condens. Matter* **35**, 333001 (2023).
- [48] T. E. Lee, “Anomalous Edge State in a Non-Hermitian Lattice,” *Phys. Rev. Lett.* **116**, 133903 (2016).
- [49] H. Hodaei, A. U. Hassan, S. Wittek, H. Garcia-Gracia, R. El-Ganainy, D. N. Christodoulides, and M. Khajavikhan, “Enhanced sensitivity at higher-order exceptional points,” *Nature* **548**, 187 (2017).
- [50] A. Ghatak and T. Das, “New topological invariants in non-Hermitian systems,” *J. Phys.: Condens. Matter* **31**, 263001 (2019).
- [51] Z. G. Yuto Ashida and M. Ueda, “Non-Hermitian physics,” *Advances in Physics* **69**, 249 (2020).
- [52] M. M. Denner, A. Skurativska, F. Schindler, M. H. Fischer, R. Thomale, T. Bzdušek, and T. Neupert, “Exceptional topological insulators,” *Nat Commun* **12**, 5681 (2021).
- [53] S. Sayyad and F. K. Kunst, “Realizing exceptional points of any order in the presence of symmetry,” *Phys. Rev. Res.* **4**, 023130 (2022).
- [54] D. Mondal and T. Nag, “Anomaly in the dynamical quantum phase transition in a non-Hermitian system with extended gapless phases,” *Phys. Rev. B* **106**, 054308 (2022).
- [55] D. Mondal and T. Nag, “Finite-temperature dynamical quantum phase transition in a non-Hermitian system,” *Phys. Rev. B* **107**, 184311 (2023).
- [56] K. Roy, K. Gogoi, and S. Basu, “Topological characterization of a non-Hermitian ladder via Floquet non-Bloch theory,” *Phys. Rev. B* **111**, 115424 (2025).
- [57] F. Dangel, M. Wagner, H. Cartarius, J. Main, and G. Wunner, “Topological invariants in dissipative extensions of the Su-Schrieffer-Heeger model,” *Phys. Rev. A* **98**, 013628 (2018).
- [58] M. van Caspel, S. E. T. Arze, and I. P. Castillo, “Dynamical signatures of topological order in the driven-dissipative Kitaev chain,” *SciPost Phys.* **6**, 026 (2019).
- [59] M. Kawasaki, K. Mochizuki, and H. Obuse, “Topological phases protected by shifted sublattice symmetry in dissipative quantum systems,” *Phys. Rev. B* **106**, 035408 (2022).
- [60] F. Yang, P. Mognini, and E. J. Bergholtz, “Dissipative boundary state preparation,” *Phys. Rev. Res.* **5**, 043229 (2023).
- [61] S. S. Hegde, T. Ehmcke, and T. Meng, “Edge-Selective Extremal Damping from Topological Heritage of Dissipative Chern Insulators,” *Phys. Rev. Lett.* **131**, 256601 (2023).
- [62] F. Song, S. Yao, and Z. Wang, “Non-Hermitian Skin Effect and Chiral Damping in Open Quantum Systems,” *Phys. Rev. Lett.* **123**, 170401 (2019).
- [63] S. Lieu, M. McGinley, and N. R. Cooper, “Tenfold Way for Quadratic Lindbladians,” *Phys. Rev. Lett.* **124**, 040401 (2020).
- [64] F. Minganti, A. Miranowicz, R. W. Chhajlany, and F. Nori, “Quantum exceptional points of non-Hermitian Hamiltonians and Liouvillians: The effects of quantum jumps,” *Phys. Rev. A* **100**, 062131 (2019).
- [65] C.-H. Liu, K. Zhang, Z. Yang, and S. Chen, “Helical damping and dynamical critical skin effect in open quantum systems,” *Phys. Rev. Res.* **2**, 043167 (2020).
- [66] T. Haga, M. Nakagawa, R. Hamazaki, and M. Ueda, “Liouvillian Skin Effect: Slowing Down of Relaxation Processes without Gap Closing,” *Phys. Rev. Lett.* **127**, 070402 (2021).
- [67] N. Okuma and M. Sato, “Quantum anomaly, non-Hermitian skin effects, and entanglement entropy in open systems,” *Phys. Rev. B* **103**, 085428 (2021).
- [68] Z. Zhou and Z. Yu, “Non-Hermitian skin effect in quadratic Lindbladian systems: An adjoint fermion approach,” *Phys. Rev. A* **106**, 032216 (2022).
- [69] F. Yang, Q.-D. Jiang, and E. J. Bergholtz, “Liouvillian skin effect in an exactly solvable model,” *Phys. Rev. Res.* **4**, 023160 (2022).
- [70] G. Lee, A. McDonald, and A. Clerk, “Anomalous large relaxation times in dissipative lattice models beyond the non-Hermitian skin effect,” *Phys. Rev. B* **108**, 064311 (2023).
- [71] K. Kawabata, T. Numasawa, and S. Ryu, “Entanglement Phase Transition Induced by the Non-Hermitian Skin Effect,” *Phys. Rev. X* **13**, 021007 (2023).
- [72] F. Yang, Z. Wei, X. Tong, K. Cao, and S.-P. Kou, “Symmetry classes of dissipative topological insulators with edge dark states,” *Phys. Rev. B* **107**, 165139 (2023).
- [73] S. Diehl, A. Micheli, A. Kantian, B. Kraus, H. P. Büchler, and P. Zoller, “Quantum states and phases in driven open

- quantum systems with cold atoms,” *Nature Phys* **4**, 878 (2008).
- [74] B. Kraus, H. P. Büchler, S. Diehl, A. Kantian, A. Micheli, and P. Zoller, “Preparation of entangled states by quantum Markov processes,” *Phys. Rev. A* **78**, 042307 (2008).
  - [75] F. Verstraete, M. M. Wolf, and J. Ignacio Cirac, “Quantum computation and quantum-state engineering driven by dissipation,” *Nature Phys* **5**, 633 (2009).
  - [76] H. Weimer, M. Müller, I. Lesanovsky, P. Zoller, and H. P. Büchler, “A Rydberg quantum simulator,” *Nature Phys* **6**, 382 (2010).
  - [77] S. Diehl, E. Rico, M. A. Baranov, and P. Zoller, “Topology by dissipation in atomic quantum wires,” *Nature Phys* **7**, 971 (2011).
  - [78] C.-E. Bardyn, M. A. Baranov, E. Rico, A. Imamoglu, P. Zoller, and S. Diehl, “Majorana Modes in Driven-Dissipative Atomic Superfluids with a Zero Chern Number,” *Phys. Rev. Lett.* **109**, 130402 (2012).
  - [79] C.-E. Bardyn, M. A. Baranov, C. V. Kraus, E. Rico, A. Imamoglu, P. Zoller, and S. Diehl, “Topology by dissipation,” *New J. Phys.* **15**, 085001 (2013).
  - [80] J. C. Budich, P. Zoller, and S. Diehl, “Dissipative preparation of Chern insulators,” *Phys. Rev. A* **91**, 042117 (2015).
  - [81] F. Iemini, D. Rossini, R. Fazio, S. Diehl, and L. Mazza, “Dissipative topological superconductors in number-conserving systems,” *Phys. Rev. B* **93**, 115113 (2016).
  - [82] A. K. Ghosh and A. M. Black-Schaffer, “Majorana zero-modes in a dissipative Rashba nanowire,” *SciPost Phys.* **17**, 036 (2024).
  - [83] H.-P. Breuer and F. Petruccione, *The theory of open quantum systems* (Oxford University Press, USA, 2002).
  - [84] G. Lindblad, “On the generators of quantum dynamical semigroups,” *Commun. Math. Phys.* **48**, 119 (1976).
  - [85] V. Gorini, A. Kossakowski, and E. C. G. Sudarshan, “Completely positive dynamical semigroups of  $N$ -level systems,” *J. Math. Phys.* **17**, 821 (1976).
  - [86] T. Prosen, “Third quantization: a general method to solve master equations for quadratic open Fermi systems,” *New J. Phys.* **10**, 043026 (2008).
  - [87] T. Prosen, “Spectral theorem for the Lindblad equation for quadratic open fermionic systems,” *J. Stat. Mech.* **2010**, P07020 (2010).
  - [88] T. Prosen and B. Žunkovič, “Exact solution of Markovian master equations for quadratic Fermi systems: thermal baths, open XY spin chains and non-equilibrium phase transition,” *New J. Phys.* **12**, 025016 (2010).
  - [89] G. T. Landi, D. Poletti, and G. Schaller, “Nonequilibrium boundary-driven quantum systems: Models, methods, and properties,” *Rev. Mod. Phys.* **94**, 045006 (2022).
  - [90] A. K. Ghosh, T. Nag, and A. Saha, “Generation of higher-order topological insulators using periodic driving,” *J. Phys.: Condens. Matter* **36**, 093001 (2023).
  - [91] A. Schnell, A. Eckardt, and S. Denisov, “Is there a Floquet Lindbladian?” *Phys. Rev. B* **101**, 100301 (2020).
  - [92] K. Kawabata, K. Shiozaki, M. Ueda, and M. Sato, “Symmetry and Topology in Non-Hermitian Physics,” *Phys. Rev. X* **9**, 041015 (2019).
  - [93] J. K. Asbóth, B. Tarasinski, and P. Delplace, “Chiral symmetry and bulk-boundary correspondence in periodically driven one-dimensional systems,” *Phys. Rev. B* **90**, 125143 (2014).
  - [94] K. Esaki, M. Sato, K. Hasebe, and M. Kohmoto, “Edge states and topological phases in non-Hermitian systems,” *Phys. Rev. B* **84**, 205128 (2011).
  - [95] L. Lin, Y. Ke, and C. Lee, “Real-space representation of the winding number for a one-dimensional chiral-symmetric topological insulator,” *Phys. Rev. B* **103**, 224208 (2021).
  - [96] K. Gogoi, T. Nag, and A. K. Ghosh, “Dissipation induced Majorana 0- and  $\pi$ -modes in a driven Rashba nanowire,” (2025).